CHEMISTRY

Bioinspired shape-memory graphene film with tunable wettability

Jie Wang, Lingyu Sun, Minhan Zou, Wei Gao, Cihui Liu, Luoran Shang, Zhongze Gu, Yuanjin Zhao*

Functional materials with specific surface wettability play an important role in a wide variety of areas. Inspired by nature's *Nepenthes* pitcher plant, we present a novel slippery film with tunable wettability based on a shape-memory graphene sponge. The porous graphene sponge coated with shape-memory polymer was used to lock in inert lubricants and construct slippery surfaces to repel different liquids. The superelasticity and high strength, together with good electrical conductivity, of the graphene sponge imparted the graphene/polymer hybrid films with fast recoverable shape-memory properties. Various droplets could slip on the compressed film with a lubricant-covered surface, but the droplets would be pinned when the shape-memory graphene film rebounded due to electrical stimulation, which caused the penetration of the infused lubricant into the pores and the exposure of rough topography film surfaces. The electrothermally dynamic tuning approach was stable and reversible; thus, the shape-memory graphene film was imparted with controlled slippery properties and functions that would be amenable to a variety of applications, such as liquid handling for microplates.

INTRODUCTION

Motivated by a broad potential impact on science and technology, materials with specific surface wettability have been the subject of intense research in areas ranging from biomedical devices and fuel transport to antifouling or anti-icing architectures (*1*–*8*). Inspired by nature's *Nepenthes* pitcher plant, lubricant-infused slippery films introduce a new paradigm for the wettability of surface materials in view of their advantages of stable and defect-free repellency for various liquids (*9*–*14*). A variety of porous materials have been used for the construction of slippery films by filling them with lubricating liquids. In particular, slippery films with tunable wettability could be achieved when the scaffolds of the porous materials are composed of elastomers, such as polydimethylsiloxane, polyurethane, and polybutadiene (*15*–*17*). By stretching these elastomer films, the infused lubricants could flow within the pores, causing the exposure of rough topography surfaces for pinning droplets. The droplets would slide down when the elastomer films are released, causing the lubricant to backflow and overcoat the surface again. Thus, slippery surfaces with tunable and programmed repellency for on-demand transportation and manipulation of liquids could be achieved (*15*). However, because of the soft structures of elastic slippery films, most of them should be fixed on tough substrates, which restricts the operation of stretching the films. In addition, even under stretching, tensile forces should be sustained to maintain the wettability states of the films; this is unrealistic and will hinder the practical application of tunable slippery films. Therefore, functional slippery films with stable, durable, easy-to-operate, and tunable wettability are still sought.

Here, we present a novel slippery film with the desired features based on a shape-memory graphene sponge. Graphene is a two-dimensional (2D) carbon sheet that has attracted interest in nearly all fields of materials science owing to its extraordinary physical and chemical properties (*18*–*20*). The 3D sponges that were derived from it also had extremely high electrical conductivity, high thermal conductivity, excellent mechanical flexibility, and a large specific surface area (*21*–*25*). Shape-memory polymers (SMPs) are a class of smart materials that can undergo programmed shape changes and return to their original shapes in response to external stimuli, such as heat and light (*26*–*28*). Thus, it is conceivable that the combination of electrothermal graphene sponges and thermally triggered SMPs with a lubricant-infused slippery stratagem would form an unprecedented material with specific wettability, as schemed in Fig. 1. The graphene sponge/SMP hybrid film with certain compression could be infused with lubricating fluids for the construction of slippery surfaces. Because of the electrothermal and shape-memory features of the film, the lubricants penetrated into the graphene sponges, and the surfaces were free of lubrication when the film recovered to its original shape under an electric field. Without the need for external forces for maintenance, the fixed shape and surface wettability of our electrothermally controllable film were stable and durable, which were different from those of the slippery elastomer films mentioned above. As a consequence of its good reversibility, fast response, and simple but persistent regulation, the lubricant-infused shape-memory graphene sponge/SMP hybrid film could be an important intelligent surface material.

RESULTS

To demonstrate the feasibility of our stratagem, the electrothermal graphene sponge was first fabricated for SMP coating and lubricant infusion. The graphene sponge was formed with the aid of in situ acrylamide (AAm) polymerization during the gelation of a graphene oxide (GO) aqueous solution. The ascorbic acid was added for the reduction of GO, accompanied by the polymerization of AAm with the help of a cross-linker [methylene-bis-acrylamide (MBAA)] and an initiator [potassium peroxydisulfate (KPS)]. The 3D graphene network was strengthened with the π-π attraction during reduction and with the hydrogen bonding formed between the amide groups in polymerized AAm chains and the hydroxyl groups of the reduced GO sheets. Both of these contributed to a more stable and ordered 3D graphene network structure, as shown in Fig. 2 (A and B). Generally, the average size of the pores of the graphene network is influenced by several parameters, including the concentration of AAm/GO, freezing temperature, and speed. Because the particular size of the pores is not necessary for encapsulating lubricants, we chose a system by random for this research. Raman spectroscopy was used to characterize the reduction of GO by providing information about the defects, chemical functionalization, and in-plane crystalline sizes. It is found that the reduced GO

State Key Laboratory of Bioelectronics, School of Biological Science and Medical Engineering, Southeast University, Nanjing 210096, China.
*Corresponding author. Email: yjzhao@seu.edu.cn

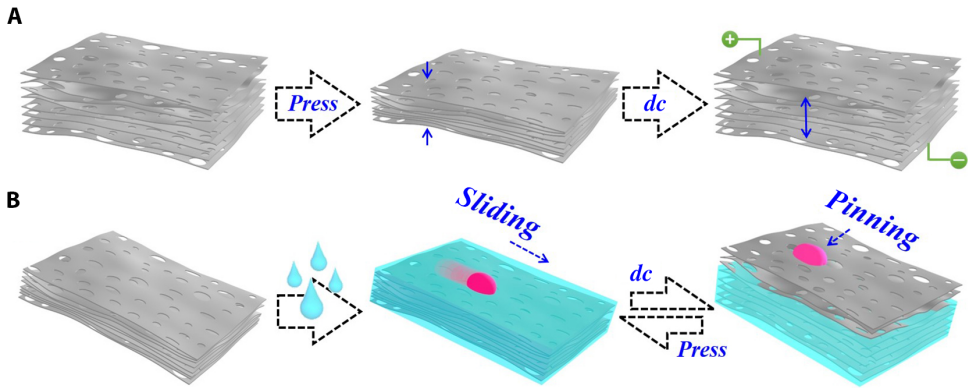

Fig. 1. Schematic diagram. Electrothermal and shape-memory graphene sponge with specific wettability. (**A**) Electrically (dc) triggered shape-memory property of the graphene sponge/SMP hybrid film. (**B**) Tunable wettability of the graphene sponge/SMP hybrid film.

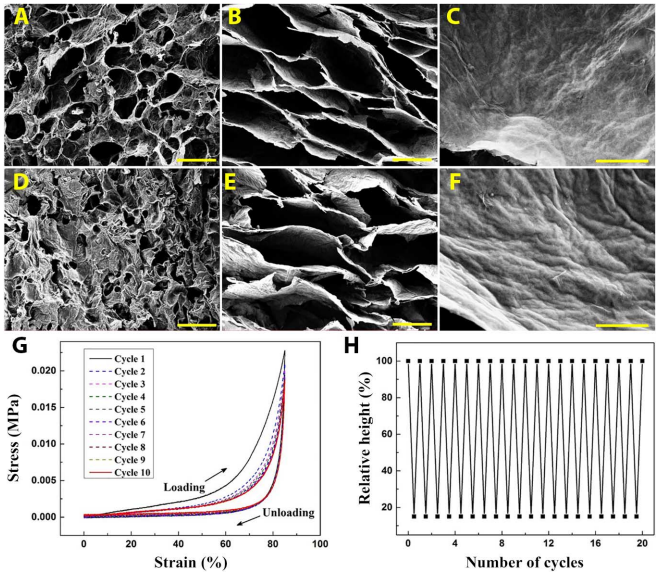

Fig. 2. Microstructures and mechanical properties. SEM images of (**A** to **C**) the graphene sponge and (**D** to **F**) the graphene/TPI hybrid sponge: (A and D) the surface; (B and E) the interior part; and (C and F) the cell walls in (B) and (E), respectively. (**G**) Compressive stress-strain curves of the graphene sponge with strains up to 85% for 10 cycles. (**H**) Height variation of the graphene/TPI hybrid sponge as a function of cycle numbers. Scale bars, 50 μm (A, B, D, and E); 5 μm (C and F).

contains typical D and G band peaks centered at 1343 and 1591 cm^{-1}, respectively, which are similar to those observed for GO (fig. S1). The I_D/I_G ratio of graphene sponge (1.15) is higher than that of GO (0.82) because of the increase in in-plane defects and the number of dangling edge atoms during the reducing process.

After preparing the reduced GO sponge, the SMP was introduced to the graphene template scaffold. *Trans*-1,4-polyisoprene (TPI) is a kind of SMP with mechanical properties affected by its crystallinity. When heated above its melting point (T_m), the crystalline TPI melts and softens to a state, which can be easily shaped under stress (*29*, *30*). As long as the shaped TPI is cooled to below its crystallization temperature (T_c), the TPI will crystallize and fix its shape (fig. S2, A and B). By heating the TPI above T_m again, it can recover to its original, stress-free state because of the elastic deformation stored during the previous step. With these unique features, the TPI was used for the fabrication of shape-memory graphene (fig. S2, C and D). The hybrid result of the graphene sponge and the SMP was investigated by scanning electron microscopy (SEM). It was found that the TPI was coated onto the surface of the graphene scaffolds, which showed apparent decreasing sizes of the remaining pores on the graphene surfaces (Fig. 2D). The interior part retained its original honeycomb-like architecture, with an average pore size of around 100 μm (Fig. 2E), whereas the cell walls of the graphene sheets were covered uniformly by the TPI, which could be confirmed from the SEM images of the graphene sheets before and after TPI coating (Fig. 2, C and F). Because of the capillary force of solvent evaporation during the introduction of TPI, the graphene/TPI hybrid sponge showed many wrinkles on its cell walls, although the porous structure of the scaffold was not damaged, which was of great importance for its mechanical properties. The thermal properties of our hybrid sponges were measured by differential scanning calorimetry (DSC) in fig. S3. As indicated in the thermograms, the concentration of the TPI contributed to the T_m and T_c values of the hybrid sponge, which made the adjustment of T_m and T_c for the hybrid sponge possible in practical applications.

Compressive tests were performed to demonstrate the compressibility of the graphene sponge and the graphene/TPI hybrid sponge. It was found that the graphene sponge was able to rapidly recover from 85% strain compression for 10 cycles of loading and unloading, and no detectable shrinkages or cracks were found after deformation, as shown in Fig. 2G and movie S1. The porous structure of the graphene sponge remained unchanged after compression, as indicated in the SEM images in fig. S4. Meanwhile, the graphene/TPI hybrid sponge also retained excellent resilience and cyclic reproducibility by the cyclic compression testing when the temperature remained above T_m (Fig. 2H and movie S2). The thickness of the hybrid material remained almost the same as its original value even after 20 cycles with strains up to 85%, indicating the repeatable and reversible compressive deformability of the hybrid sponge. Note that even after 5000 cycles of compression with a temperature above T_m, the relative height of the hybrid sponge could still remain about 89.7% (fig. S5A). This excellent mechanical property was ascribed to the contribution of polymerized AAm chains and reduced GO sheets (fig. S5B and table S1). It was found that the hybrid sponges with polymerized AAm presented much better mechanical properties than the sponge without AAm, and the high concentration of AAm had no obvious influence on improving the mechanical property, whereas the mechanical property of the hybrid sponges showed a positive association with the GO concentration, which determined the scaffold strength of the sponge.

The shape-memory property of the TPI caused the graphene/TPI hybrid sponge to fix its shape by cooling to T_c. Thus, the thickness of the sponge could be controlled under different stress values with the help of TPI crystallization (Fig. 3), in which case the 3D pore structure of the graphene scaffold would change with size. However, the sponge thickness was out of control when the sponge was compressed at room temperature because of the unused TPI shape-memory crystallization (fig. S6). Although coated with the TPI, the conductive network of the graphene/TPI hybrid sponge was not damaged. Thus, it allowed uniform heat transmission throughout the sponge structure. As detected in fig. S7, when the resistance of the sponge began to change, the corresponding temperature was about 56°C, which was consistent with the T_m of the hybrid sponge. In addition, with the thickness changes of the sponge under heating from 30° to 115°C, the resistance of the graphene/TPI hybrid sponge increased from 10 to 23 ohms, indicating that the shape-memory hybrid sponge had good electrical conductivity and electrothermal properties. Benefitting from the features of superelasticity, shape memory, and good electrical/electrothermal conductivity, the graphene/TPI hybrid sponge was imparted with fast recoverable electro-induced shape-memory properties.

To construct the slippery surface, the lubricating fluid, such as perfluorinated oil (DuPont Krytox 103), was infused into the 3D microscale pore structure of a graphene/TPI hybrid film and even overcoated the surface. To convert the microstructured surfaces into low surface energy materials that can stably contain the fluorinated lubricant, we treated the hybrid film with a fluorinated reagent using 1*H*,1*H*,2*H*,2*H*-perfluorooctyltrichlorosilane. After this treatment, the infusion of the lubricant into the porous structure of the film was easy to achieve. Because of the low surface energy of the selected lubricant, the surface of the hybrid graphene film was physically smooth to the molecular scale and could repel liquids. It was found that the water droplet contact angle on the surface infused with lubricant became 93.64° from its original 111.65° without lubricant filling (fig. S8, A and C), and the oil contact angle (for silicone oil) became 35.63° from its original 0° (fig. S8, B and D). Aside from the effect on the contact angle, filling the film with perfluorinated oil also led to significant changes in the sliding angle of the droplets on the surfaces of the films (Fig. 4, A and B). It could be observed that the water droplets were pinned on the porous rough surface and the sliding angle hysteresis of the droplets on this situation trended toward infinity when the film was not filled with the perfluorinated oil (Fig. 4A). However, with the presence of the perfluorinated oil, the sliding angle of the droplet was only 2°, which demonstrated excellent slippery properties for water (Fig. 4B). The wettability of the graphene sponge film without TPI was also investigated in fig. S9, which presented a similar droplet pinning feature without the lubricants' infusion and the similar repellence for droplets when coated with perfluorinated oil.

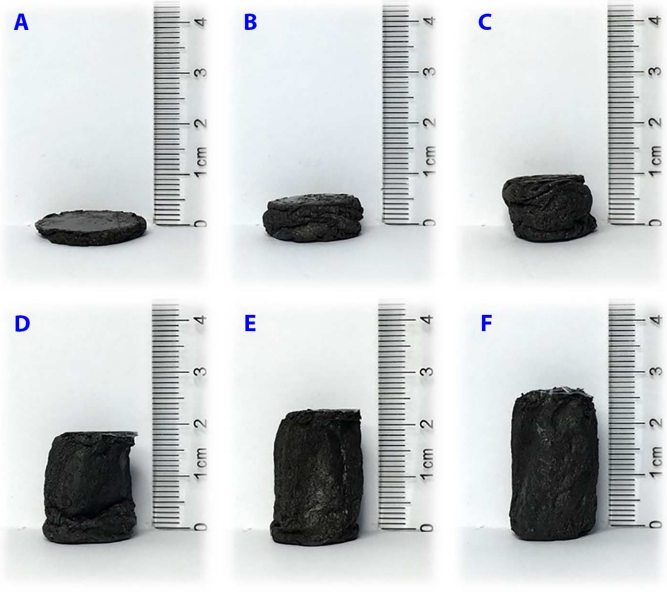

Fig. 3. Appearances of the hybrid sponge. Appearances of the shape-memory graphene/TPI hybrid sponge with fixed shapes and designed heights. The sponge was tailored to different thicknesses under stress (from about 10 to 100%), which was fixed by cooling it below T_c.

Note that the surface of the graphene/TPI hybrid sponge film could repel immiscible liquids of virtually any surface tension, which was confirmed by recording the contact angles and sliding angles of the surface (Fig. 4C). The hybrid film exhibited extreme liquid repellence, as signified by very low sliding angles (less than 5°) against liquids with surface tension ranging from 18.43 mN m^{-1} (pentane) to 72.4 mN m^{-1} (water). These low values of the sliding angle directly indicated low resistance for droplet motion, which confirms a lack of pinning and the nearly defect-free surface of the system. Therefore, the lubricating fluid-infused graphene/TPI hybrid film provided an ideal slippery surface.

The electro-induced shape-memory property of the graphene/TPI hybrid film provided a promising means to dynamically manipulate the mobility of both oil and water droplets on the surface. As mentioned above, the thickness of the graphene scaffold could be tuned under different stresses and could recover to its original, stress-free condition. Thus, when a constant dc voltage was applied to the compressed film infused with lubricating fluids, a large amount of heat was generated immediately and transmitted to the entire sample, resulting in the rebounding of the film. Because the configuration of the lubricating fluid is limited by its volume, substrate morphology, topography, and space accessible for infiltration, the lubricant could penetrate into the pores, leaving the surface layer free of lubrication. The resultant rough surface morphology of the shape-memory graphene/TPI hybrid film would prevent the droplets from slipping and would pin them on its surface. Thus, the dynamic gas-liquid-solid interface provided by the graphene hybrid film could reversibly transit between a lubricant-coated surface and a textured roughness surface in response to electrical stimuli sensed by the elastic substrate.

To demonstrate this tuning function, we analyzed the dynamic wettability of the hybrid film by monitoring the liquid droplets on the surface of the shape-memory graphene/TPI hybrid film, as shown in Fig. 5 and movie S3. It could be found that, under compressed conditions, the droplets rapidly slid down the liquid-infused graphene substrate (Fig. 5A) but stopped and were held in place when a constant dc voltage was applied to the substrate (Fig. 5C). This novel material, with on-demand tunable repellency, paves the way for active microfluidics and liquid harvesting, transport, and manipulation technologies.

As a typical application example of the shape-memory graphene/TPI hybrid film, we used it for the liquid handling for microplates. Microplate technology has been accepted as the most reliable platform for biomedical areas. One of the main challenges associated with microplate technology is that it requires a large number of steps for pipetting different liquids into each well, which is time-consuming and labor-intensive. Thus, we suggested a graphene/TPI hybrid film array (fig. S10) with electrothermally controlled surface wettability in each independent unit for accurately pipetting liquids to the microplates, as schemed in

Fig. 6A. The compressed graphene/TPI hybrid film array with a lubricant-covered surface was still able to repel various sample liquids, with no residues similar as those of the above integrated film. However, when an electrical stimulation was applied on the marginal unit of the compressed film array, the rhomboid graphene/TPI hybrid material unit returned to its original shape; thus, the slide path of the liquid droplets was blocked and shifted to the desired well of the microplate along the edge of the raised graphene/TPI hybrid unit, as shown in Fig. 6B. With programmed electrical stimulation of each unit of the graphene/TPI hybrid film array, the slide path of the liquid droplets could turn to the corresponding wells of the microplate (Fig. 6B, ii and iii). Because no liquid was residual on the surface of the graphene/TPI hybrid film array, it was able to pipette different samples into different wells of the microplate, as shown in Fig. 6C. Besides, the hybrid film array could also be used to achieve gradient concentrations of samples in the microplate wells by controlling the kinds and ratios of the sliding sample droplets

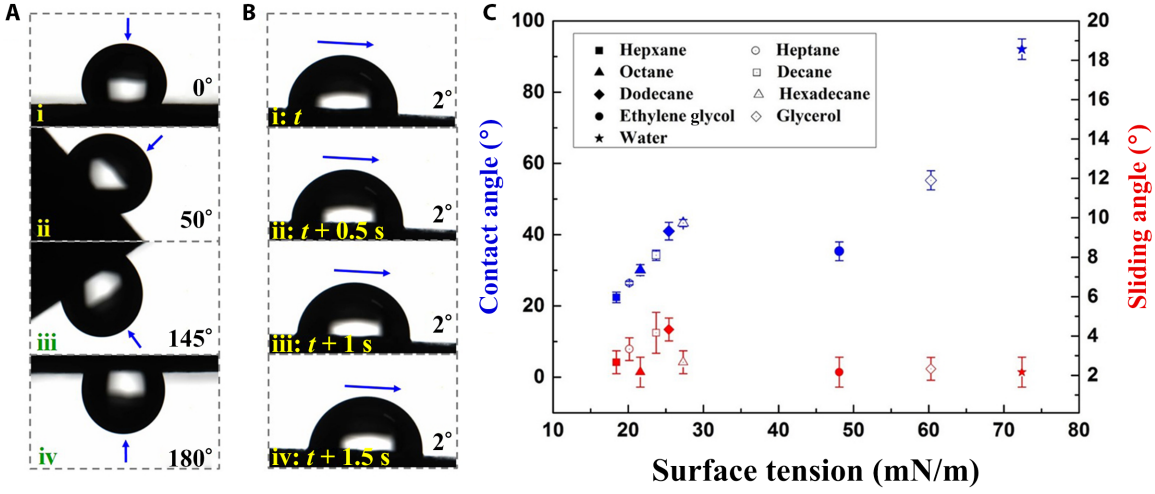

Fig. 4. Wettability results. (**A**) Appearances of the water droplet pinned on the surface of the graphene/TPI hybrid film without infusing perfluorinated oil; the surface tilted from 0° to 180°. (**B**) Progress of the water droplet sliding down the surface of the graphene/TPI hybrid film with perfluorinated oil filling (sliding angle, 2°). Images (ii), (iii), and (iv) were taken 0.5, 1, and 1.5 s, respectively, after the first image of (i) in (B). (**C**) Comparison of contact angles and sliding angles as a function of surface tension of test liquids on the film. Contact angles of liquids in homolog series linearly increased with increasing surface tensions. Error bars indicate SDs from five independent measurements.

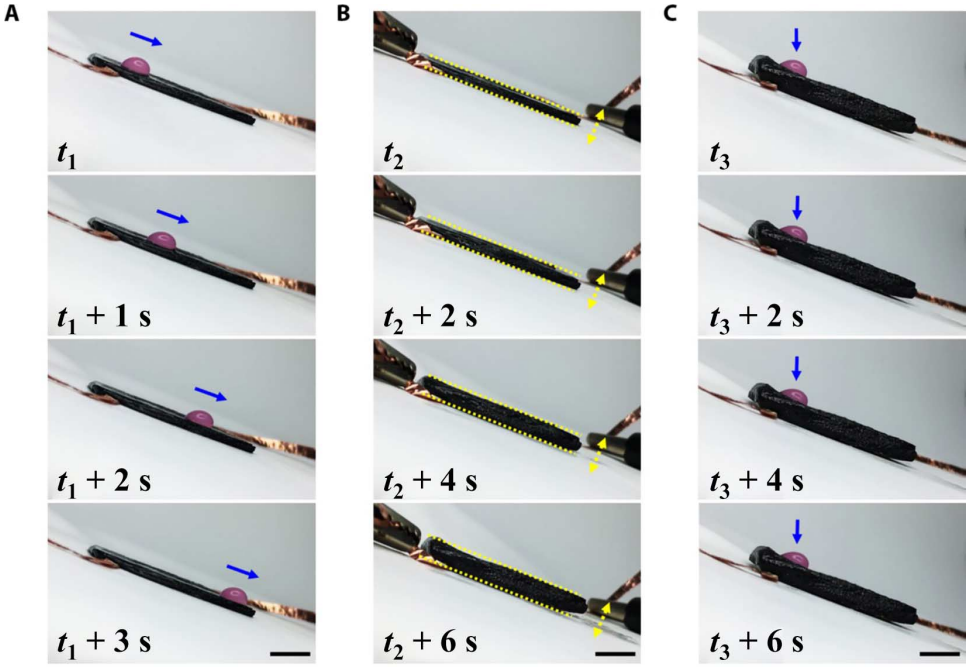

Fig. 5. Dynamic control of droplet mobility on a tilted surface. (**A**) Progress of a water droplet sliding down the surface of the compressed graphene/TPI film with perfluorinated oil filling. (**B**) Progress of the film recovering to its original shape in a few seconds when applied with dc voltage (6 V). (**C**) Progress of the droplet pinned on the film surface after electrical stimulation. Graphene/TPI film of a random thickness could show similar tunable wettability. Time differences of the images taken from the first images in (A) to (C) are shown in corresponding images. Scale bars, 1 cm.

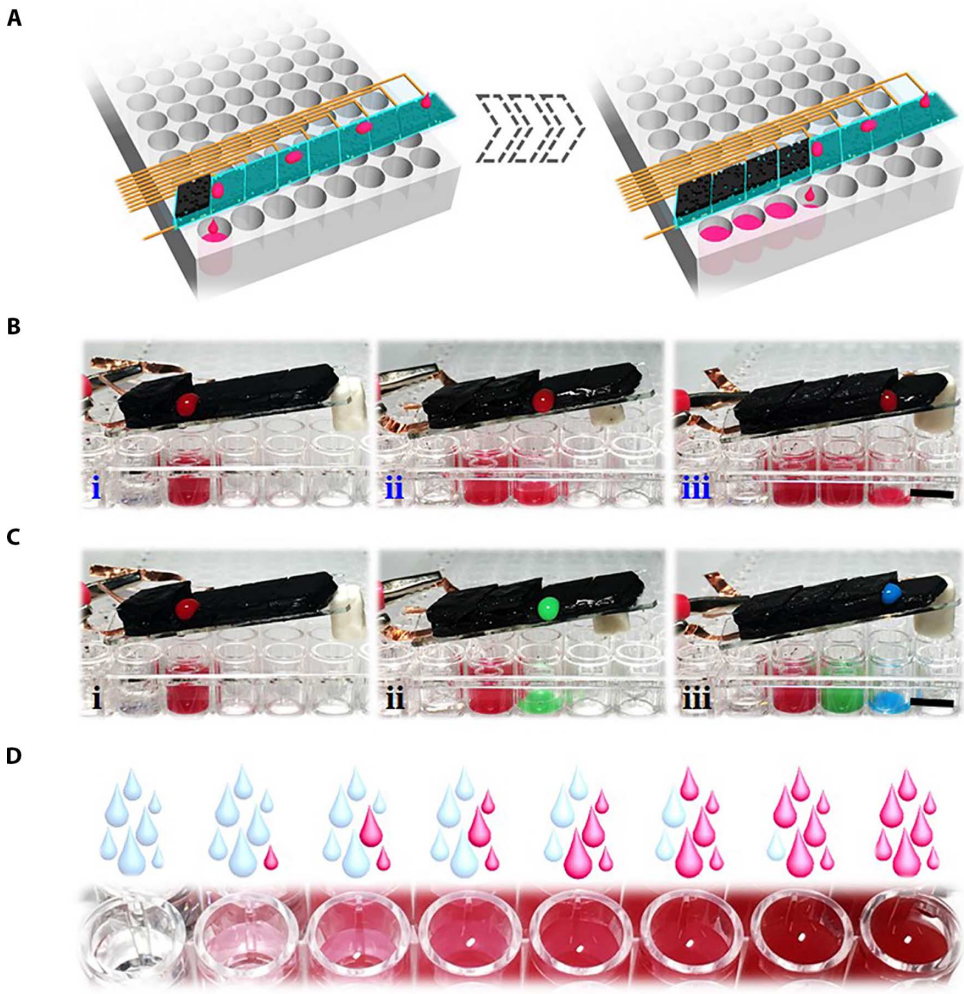

Fig. 6. Graphene/TPI hybrid film array for pipetting droplets to microplates. Schematic diagram (**A**) and images (**B** and **C**) of the progress of applying the graphene/TPI hybrid film array for pipetting droplets into microplates. Same samples were pipetted into different wells in (B), and different samples were pipetted into different wells in (C). (**D**) Gradient concentrations of samples in the microplate wells were achieved by controlling the kinds and ratios of the sliding sample droplets. Scale bars, 1 cm (B and C).

(Fig. 6D). These features of the shape-memory graphene/TPI hybrid film array indicate its potential values in biomedical areas.

DISCUSSION

We have demonstrated a novel bioinspired shape-memory graphene film with electrothermally controlled surface wettability. The film was made of a graphene/TPI hybrid porous structure material, which could be used to lock in the infused lubricant and construct a slippery surface to repel various liquids. With the shape-memory function in response to electric fields, the lubricant could infiltrate into the pores when the film recovered to its original shape, leaving the surface layer free of lubrication, and thus pinned droplets of liquids along the surface. As the electrothermally dynamic surface wettability was stable and reversible, the shape-memory graphene/TPI hybrid film was imparted with controlled slippery properties and functions that would be amenable to a variety of applications.

Similar to traditional slippery surfaces, our bioinspired slippery surface is also aimed at repelling various liquids with different surface tensions, which will introduce a new paradigm for materials capable of meeting emerging needs in a range of energy, environmental, and biomedical applications that require long-term operations and encounter harsh environmental conditions. However, different from previous methods, which have some fundamental limitations, such as constant wettability for solid substrates, low robustness, requirement of sustained forces, and shape resilience for elastic substrates, our slippery surface is based on shape-memory graphene spongy film; thus, it has tunable and programmed repellency for on-demand transportation and manipulation of liquids, which is stable, durable, and easy to operate.

For liquid handling, multichannel pipettes or automatic microarrayers can also distribute different samples into different wells of microplates. However, the original samples for the multichannel pipettes or automatic microarrayers still need to be prepared one by one. Also, large numbers of pipette tips or pins are consumed to save pipetting steps and avoid sample pollution. In addition, complex equipment and expert skills are usually required to run an automatic microarrayer in high-throughput sample distribution. In contrast, without the requirements of preparing original samples one by one, consuming pipette tips or

pins, and using precise devices to move the samples, our method can distribute the sample droplets to effective addresses of the microplates by controlling a circuit, which greatly simplifies the liquid handling process. Moreover, using parallel graphene/TPI hybrid film arrays with lubricant-covered surfaces, it is possible to achieve high-throughput liquid handling for the whole microplate. Furthermore, because the hybrid film arrays are shape memory materials, they can be reused for liquid handling by compressing, which decreases the cost of our technology. In conclusion, it can be envisioned that our shape-memory graphene surface will be expanded to conduct a large number of additional applications, such as liquid harvesting devices, microfluidic channels, medical instruments, and liquid handling robotic systems.

MATERIALS AND METHODS

Materials

The GO solution was bought from Nanjing XFNANO Materials Tech Co. Ltd. AAm and KPS were obtained from Aladdin Industrial Corporation. MBAA and ascorbic acid were purchased from Sinopharm Chemical Reagent Co. Ltd. 1*H*,1*H*,2*H*,2*H*-Perfluorooctyltrichlorosilane was obtained from Shanghai Macklin Biochemical Co. Ltd. TPI and dicumyl peroxide (DCP) were provided by Sigma-Aldrich Co. The perfluorinated oil (Krytox 103) was bought from DuPont Performance Lubricants.

Fabrication of the graphene sponge

Designated amounts of AAm, MBAA, KPS, and ascorbic acid were added to the GO solution at certain concentrations. For a typical experiment, ascorbic acid (150 mg), AAm (75 mg), MBAA (3.3 mg), and KPS (0.6 mg) were added to the GO solution (10 ml; concentration, 7.5 mg ml^{-1}) under stirring at ice-water temperature for 2 hours. The mixed solution was then bubbled with nitrogen gas for at least 30 min in a sealed Teflon container and placed in a water bath (90°C) for 6 min to partially reduce GO. To strengthen the π-π attraction between partial reduced GO (pr-GO) sheets and the hydrogen bonding formed between the amide groups in poly(AAm) (PAAm) chains, we placed the container on the shelf of the freeze dryer for 1 hour and then thawed it at room temperature. After this, the sample was reduced at 70°C for 20 hours for the enhancement of π-π attraction. The resultant graphene/PAAm hydrogels were subjected to dialysis in deionized water for at least 48 hours to remove the free PAAm and unreacted chemicals. After the hydrogel was freeze-dried, the sample was further annealed at 180°C for 2 hours. The shape of the sealed container decided the final shape of the graphene aerogel foam. Sealed cylinder and cuboid Teflon containers were used in our experiment to fabricate graphene foams and films.

Fabrication of the graphene/TPI hybrid sponge

TPI and a cross-linking agent (DCP) were added at a weight ratio of 100:2 to chloroform at a concentration of 20 mg ml^{-1}. The fabricated graphene aerogel foam was immersed in the polymer solution for 30 min and was then air-dried at room temperature. The sample was then heated at 160°C under nitrogen for 15 min to induce the cross-linking reaction, resulting in the production of graphene/TPI hybrid foam. To convert the sample surfaces into low surface energy materials and stably contain the fluorinated lubricant, we immersed the hybrid sample in the 1*H*,1*H*,2*H*,2*H*-perfluorooctyltrichlorosilane solution overnight and washed it with ethyl alcohol solution. For compressing the hybrid sponges to different heights, different values of pressure were required. The critical pressure to compress a cylindrical hybrid sponge without TPI, with TPI, and with TPI/lubricant (with a diameter of 10 mm and a height of 5 mm) to 85% of original height was about 85*g*, 116*g*, and 121*g*, respectively.

Liquid lubrication and electrically induced shape-memory slippery test

Krytox 103 was added to the substrate, and uniform coverage was achieved by tilting. Water was dyed to make the slippery test observable. A constant dc voltage (6 V) was applied to the graphene/TPI hybrid film to observe its electro-induced shape-memory behavior.

Fabrication of the graphene/TPI hybrid film array and application for pipetting

The graphene/TPI hybrid film array was composed of adjacent rhomboid graphene/TPI hybrid films with sharp and smooth edges, as well as tiny spaces between each film. The spaces were important in guaranteeing the nonconduction between adjacent films and required to make the lubricants overcoat the whole array with a slippery surface at the same time. In our experiment, film units were designed with a length and width of 9 mm on a tilted glass to pipette accurately for 96-well microplates. The films had independent conductive circuits, which were determined by the different copper wires. Note that the copper wire belonging to one film was put away from the upstream film in the direction of the liquids that slid down, to decrease the heat influence of the upstream film. The length of the film units was nearly the same as the diameter of the wells of the microplates, and the vertexes of the graphene rhomboids were put in the center of the wells to enable accurate falling of the liquids. Water was dyed with red, green, and blue to make the pipetting tests observable. A constant dc voltage (6 V) was applied to alter the slide path.

Characterization

SEM images were obtained using an SEM (Hitachi S-3000N). Color photos and videos were taken on a digital camera (Canon 5D Mark II). Raman spectroscopy was conducted using a Raman microscope (RAMAN, inVia, Renishaw) with a 532-nm laser to analyze the surface physicochemical structure of the products. The mechanical strength of the graphene aerogel foam was tested using an Instron 5943 single-column testing machine (ITW) with a load cell capacity of 1 kN. The loading process was displacement-controlled, and the loading rate was set to be 3 mm min^{-1}. DSC thermograms were measured using DSC 8000 (PerkinElmer), with second heating curves and cooling curves at heating and cooling rates of 10°C min^{-1}. The resistance of the graphene foam was measured by a semiconductor characterization system (4200-SCS/F, Keithley). Water contact angles were obtained by a JC2000D2 contact angle measuring system at ambient temperature. Sliding angles were measured on a customized tilting stage with a droplet volume of 6 μl. Static contact angles were recorded with a droplet volume of 2 μl. The static contact angles were measured at a neutral tilting angle (0°). The tested liquids were hexane (18.43 mN m^{-1}), heptane (20.14 mN m^{-1}), octane (21.6 mN m^{-1}), decane (23.7 mN m^{-1}), dodecane (25.4 mN m^{-1}), hexadecane (27.3 mN m^{-1}), ethylene glycol (48.1 mN m^{-1}), glycerol (60.3 mN m^{-1}), and water (72.4 mN m^{-1}).

SUPPLEMETARY MATERIALS

Supplementary material for this article is available at http://advances.sciencemag.org/cgi/content/full/3/6/e1700004/DC1

fig. S1. Raman spectra of GO and reduced GO of the sponge.

fig. S2. SEM images of pure TPI, and the photos of the graphene sponge and the graphene/TPI hybrid sponge.

fig. S3. DSC thermograms of TPI, the hybrid sponge without TPI, and the hybrid sponge with different concentrations of TPI.
fig. S4. SEM images of the graphene sponge before and after 10 cycles' compression.
fig. S5. The mechanical properties of graphene/TPI hybrid sponges.
fig. S6. The photos of graphene/TPI hybrid sponge before, under, and after compression at room temperature.
fig. S7. The resistance and temperature of a cylindrical graphene/TPI hybrid sponge as a function of time.
fig. S8. The wettability of the graphene/TPI hybrid film with and without perfluorinated oil.
fig. S9. The dynamic control of droplet mobility on a tilted graphene sponge film.
fig. S10. The schematic diagram and the photo of the hybrid graphene film array with four units.
table S1. Compositions of initial aqueous solutions used for preparing hybrid sponges with different concentrations of GO (G) and AAm (P).
movie S1. Compressive tests of the graphene sponge for 10 cycles.
movie S2. Compressive tests of the graphene/TPI hybrid sponge for 10 cycles at 100°C.
movie S3. Dynamic wettability of the graphene/TPI hybrid film by monitoring the liquid droplets on the slippery surface shown in Fig. 5.

REFERENCES AND NOTES

1. L. P. Wen, Y. Tian, L. Jiang, Bioinspired super-wettability from fundamental research to practical applications. *Angew. Chem. Int. Ed.* **54**, 3387–3399 (2015).
2. B. Su, Y. Tian, L. Jiang, Bioinspired interfaces with superwettability: From materials to chemistry. *J. Am. Chem. Soc.* **138**, 1727–1748 (2016).
3. Y. J. Zhao, H. C. Gu, Z. Y. Xie, H. C. Shum, B. P. Wang, Z. Z. Gu, Bioinspired multifunctional Janus particles for droplet manipulation. *J. Am. Chem. Soc.* **135**, 54–57 (2013).
4. H. L. Li, J. X. Wang, L. M. Yang, Y. L. Song, Superoleophilic and superhydrophobic inverse opals for oil sensors. *Adv. Funct. Mater.* **18**, 3258–3264 (2008).
5. S.-H. Kim, A. Abbaspourrad, D. A. Weitz, Amphiphilic crescent-moon-shaped microparticles formed by selective adsorption of colloids. *J. Am. Chem. Soc.* **133**, 5516–5524 (2011).
6. J. Wang, L. R. Shang, Y. Cheng, H. B. Ding, Y. J. Zhao, Z. Z. Gu, Microfluidic generation of spongy graphene encapsulated porous particles for oil absorption. *Small* **11**, 3890–3895 (2015).
7. W. Q. Feng, L. X. Li, X. Du, A. Welle, P. A. Levkin, Single-step fabrication of high-density microdroplet arrays of low-surface-tension liquids. *Adv. Mater.* **28**, 3202–3208 (2016).
8. J. Wang, Y. Zhang, S. Wang, Y. Song, L. Jiang, Bioinspired colloidal photonic crystals with controllable wettability. *Acc. Chem. Res.* **44**, 405–415 (2011).
9. T.-S. Wong, S. H. Kang, S. K. Y. Tang, E. J. Smythe, B. D. Hatton, A. Grinthal, J. Aizenberg, Bioinspired self-repairing slippery surfaces with pressure-stable omniphobicity. *Nature* **477**, 443–447 (2011).
10. Y. Tian, B. Su, L. Jiang, Interfacial material system exhibiting superwettability. *Adv. Mater.* **26**, 6872–6897 (2014).
11. N. Vogel, R. A. Belisle, B. Hatton, T.-S. Wong, J. Aizenberg, Transparency and damage tolerance of patternable omniphobic lubricated surfaces based on inverse colloidal monolayers. *Nat. Commun.* **4**, 2176 (2013).
12. K.-C. Park, P. Kim, A. Grinthal, N. He, D. Fox, J. C. Weaver, J. Aizenberg, Condensation on slippery asymmetric bumps. *Nature* **531**, 78–82 (2016).
13. I. You, T. G. Lee, Y. S. Nam, H. Lee, Fabrication of a micro-omnifluidic device by omniphilic/omniphobic patterning on nanostructured surfaces. *ACS Nano* **8**, 9016–9024 (2014).
14. K. R. Phillips, G. T. England, S. Sunny, E. Shirman, T. Shirman, N. Vogel, J. Aizenberg, A colloidoscope of colloid-based porous materials and their uses. *Chem. Soc. Rev.* **45**, 281–322 (2016).
15. J. Kamei, H. Yabu, On-demand liquid transportation using bioinspired omniphobic lubricated surfaces based on self-organized honeycomb and pincushion films. *Adv. Funct. Mater.* **25**, 4195–4201 (2015).
16. C. Liu, H. Ding, Z. Wu, B. Gao, F. Fu, L. Shang, Z. Gu, Y. Zhao, Tunable structural color surfaces with visually self-reporting wettability. *Adv. Funct. Mater.* **26**, 7937–7942 (2016).
17. X. Yao, Y. H. Hu, A. Grinthal, T.-S. Wong, L. Mahadevan, J. Aizenberg, Adaptive fluid-infused porous films with tunable transparency and wettability. *Nat. Mater.* **12**, 529–534 (2013).
18. K. Yan, L. Fu, H. Peng, Z. Liu, Designed CVD growth of graphene via process engineering. *Acc. Chem. Res.* **46**, 2263–2274 (2013).
19. L. Zhang, J. Yu, M. Yang, Q. Xie, H. Peng, Z. Liu, Janus graphene from asymmetric two-dimensional chemistry. *Nat. Commun.* **4**, 1443 (2013).
20. Q. Zhou, G. Shi, Conducting polymer-based catalysts. *J. Am. Chem. Soc.* **138**, 2868–2876 (2016).
21. B. Yao, J. Chen, L. Huang, Q. Zhou, G. Shi, Base-induced liquid crystals of graphene oxide for preparing elastic graphene foams with long-range ordered microstructures. *Adv. Mater.* **28**, 1623–1629 (2016).
22. C. Cheng, D. Wang, Hydrogel-assisted transfer of graphene oxides into nonpolar organic media for oil decontamination. *Angew. Chem. Int. Ed.* **55**, 6853–6857 (2016).
23. X. Xu, Q. Zhang, Y. Yu, W. Chen, H. Hu, H. Li, Naturally dried graphene aerogels with superelasticity and tunable Poisson's ratio. *Adv. Mater.* **28**, 9223–9230 (2016).
24. X. Gao, J. Zhou, R. Du, Z. Xie, S. Deng, R. Liu, Z. Liu, J. Zhang, Robust superhydrophobic foam: A graphdiyne-based hierarchical architecture for oil/water separation. *Adv. Mater.* **28**, 168–173 (2016).
25. Y. Xu, G. Shi, X. Duan, Self-assembled three-dimensional graphene macrostructures: Synthesis and applications in supercapacitors. *Acc. Chem. Res.* **48**, 1666–1675 (2015).
26. D. Zhang, K. M. Petersen, M. A. Grunlan, Inorganic–organic shape memory polymer (SMP) foams with highly tunable properties. *ACS Appl. Mater. Interfaces* **5**, 186–191 (2013).
27. I. Gurevitch, M. S. Silverstein, Shape memory polymer foams from emulsion templating. *Soft Matter* **8**, 10378–10387 (2012).
28. H. B. Nejad, R. M. Baker, P. T. Mather, Preparation and characterization of triple shape memory composite foams. *Soft Matter* **10**, 8066–8074 (2014).
29. T. Tsujimoto, K. Toshimitsu, H. Uyama, S. Takenob, Y. Nakazawa, Maleated *trans*-1,4-polyisoprene from *Eucommia ulmoides* Oliver with dynamic network structure and its shape memory property. *Polymer* **55**, 6488–6493 (2014).
30. H. Sun, F. Zhao, P. He, S. Zhao, Influence of amount of sulfur on mechanical, dynamic, and shape-memory properties of trans-1,4-polyisoprene. *J. Macromol. Sci. B* **50**, 871–879 (2011).

Acknowledgments
Funding: This work was supported by the National Science Foundation of China (grant nos. 21473029 and 51522302), the NSAF Foundation of China (grant no. U1530260), the National Science Foundation of Jiangsu (grant no. BK20140028), the 111 Project (grant no. B17011), the Program for New Century Excellent Talents in University, the Scientific Research Foundation of Southeast University, and the Scientific Research Foundation of Graduate School of Southeast University. **Author contributions:** Y.Z. conceived the idea and designed the experiment; J.W. carried out the experiments; J.W. and Y.Z. analyzed the data and wrote the paper; L. Sun and M.Z. assisted with experiment operations; W.G., C.L., L. Shang, and Z.G. contributed to scientific discussion of the article. **Competing interests:** The authors declare that they have no competing interests. **Data and materials availability:** All data needed to evaluate the conclusions in the paper are present in the paper and/or the Supplementary Materials. Additional data related to this paper may be requested from the authors.

Submitted 2 January 2017
Accepted 6 April 2017
Published 2 June 2017
10.1126/sciadv.1700004

Citation: J. Wang, L. Sun, M. Zou, W. Gao, C. Liu, L. Shang, Z. Gu, Y. Zhao, Bioinspired shape-memory graphene film with tunable wettability. *Sci. Adv.* **3**, e1700004 (2017).